

## Anderson localization of light: Strong dependence with incident angle

*Ernesto Jimenez-Villar<sup>1\*</sup>, M.C. S. Xavier<sup>2,3</sup>, Valdeci Mestre<sup>4</sup>, Weliton S. Martins<sup>5</sup>, Gabriel F. Basso<sup>6</sup>, Gilberto F. de Sá<sup>1</sup>*

<sup>1</sup>Departamento de Química Fundamental, Universidade Federal de Pernambuco, Recife, PE 50670-901, Brazil

<sup>2</sup>Departamento de Física, Universidade Federal da Paraíba, João Pessoa, PB 58051-970, Brazil

<sup>3</sup>Departamento de Física, Universidade Estadual da Paraíba, Araruna, PB 58233-000, Brazil

<sup>4</sup>CCEA, Universidade Estadual da Paraíba, Patos, PB 58706-560, Brazil

<sup>5</sup>Departamento de Física, Universidade Federal Rural de Pernambuco, Recife PE 52171-900, Brazil

<sup>6</sup>Departamento de Informática, Universidade Federal da Paraíba, Joao Pessoa PB 58055-000, Brazil

E-mail: Ernesto.Jimenez@uv.es

Keywords: Localization of light, Photonics in disordered media, Mirror-symmetry breaking, Strongly disordered optical media, Core-shell nanoparticles

### Abstract:

Anderson localization of light and associated phenomena has greatly attracted the attention of researchers in the past few decades. This paper studies the transport of light for different incidence angles in a strongly disordered optical medium composed by core-shell nanoparticles (TiO<sub>2</sub>@Silica) suspended in ethanol solution. A decrease of optical conductance and an increase of absorbed energy are reported when the incidence angle is increased. This phenomenon was associated to the large increase of internal reflection with the incidence angle, which is a direct consequence of the enhanced refractive index near the input surface by localization. The specular reflection, measured for the photons that enter the sample, is considerably lower than the effective internal reflection undergone by the coherently backscattered photons in the exactly opposite direction, indicating a non-reciprocal propagation of light (mirror-symmetry breaking). This study represents a novel approach in order to understand the complex physics involved in a disordered optical medium at the critical regime of localization.

### Introduction:

Anderson localization of light<sup>1, 2, 3, 4</sup> is an open research frontier. Various pioneering

experiments that studied the transmission of electromagnetic waves through strongly disordered optical media have claimed the observation of localization of light.<sup>5,6,7</sup> However, these works were questioned firstly by opponents<sup>8,9</sup> and later refuted by their authors.<sup>10,11</sup> The inelastic scattering processes (absorption or nonlinearity) can lead to a decrease in the photon coherence length, hampering the interference effects (localization).<sup>1,12</sup> Indeed, according to the theoretical prediction of Sajeev John<sup>1</sup> and our previous experimental results,<sup>13</sup> an enhanced absorption arises when the system approaches localization. In this previous work,<sup>13</sup> we reported several pieces of experimental evidence of localization transition in a strongly disordered optical medium composed by TiO<sub>2</sub>@Silica nanoparticles (NPs) in ethanol solution. By using a Stöber method,<sup>14,15</sup> TiO<sub>2</sub> NPs were coated with a homogeneous silica shell of ~40 nm thickness. The silica coating with thicknesses around or above 40 nm prevents the “optical” junction of the TiO<sub>2</sub> scattering surfaces (steric “optical” effect),<sup>16</sup> decreasing considerably the near-field coupling, which decreases the scattering strength<sup>17</sup> and could hamper localization.<sup>18</sup> We called this property optical colloidal stability.<sup>16</sup> In addition, the silica shell provides a light-coupling enhancement with TiO<sub>2</sub> scatter cores,<sup>17</sup> inertness,<sup>19,20</sup> and high dispersibility<sup>21,22,23</sup> which has enabled their use in numerous applications.<sup>24,25,26</sup> Transport experiments in this strongly disordered optical medium (TiO<sub>2</sub>@Silica) showed an enhanced absorption near the input border when the system approached localization, from which an increase of refractive index was proposed. This enhancement of absorption and refractive index was interpreted as that localized photons interact several times with the same particles, molecules or atoms (localized states). This means that the effective refractive index (internal reflection) that the localized photons would feel, would be higher than that felt by the photons that enter the sample (non-localized photons). The enhancement of refractive index near the input border ( $n_{\text{eff0}}$ ) by localization (successive elastic polarization of valence electrons to virtual states) finds a parallel in the dynamic barrier proposed by Campagnano

and Nazarov<sup>27</sup> in the border of a disordered electronic medium. This could be understood like a photon accumulation near the input border, due to localization increase in the vicinity of the boundary, which was theoretically predicted by Mirlin in disordered electronic media.<sup>28,29</sup> An increase of the internal reflection (refractive index) must force the photons path to be longer. Consequently, the likelihood of interference should increase (localization increase). This issue was addressed theoretically by Ramos and co-workers,<sup>30</sup> who demonstrated that the presence of a finite barrier (internal reflection) in the border provokes an increase of the quantum interference in a disordered electronic medium (localization). Thereby, a decrease of the optical conductance would be expected when the incidence angle (internal reflection) increases. Clearly, this effect would only be appreciable if the effective refractive index near the input border is largely enhanced by localization. For diffusive regime (classical refractive index), very low percentage of coherently backscattered photons (previously localized) and low contrast between the refractive indexes at the input interface (silica cuvette and sample, 1.46-1.53), the internal reflection for the photons leaving the sample (backscattered) would hardly change with the incidence angle (<1%). In this paper, experiments of total and inelastic transmission, photon cloud propagation and coherent backscattering were performed, demonstrating strong influence of the incidence angle over localization (optical conductance) and associated phenomena (absorption).

## **Materials and methods**

### *Sample preparation*

TiO<sub>2</sub>@Silica NPs with a homogeneous silica shell of ~40 nm thickness, synthesized by an improved strobe method,<sup>14,15</sup> were dispersed in ethanol solution at [140x10<sup>10</sup> NPs ml<sup>-1</sup>].

### *Transmission experiments:*

For all experiments, a CW He-Ne laser, linearly polarized with polarization parallel to incidence plane, model Uniphase 1125P (10 mW, 633 nm) was used. Total transmission is

measured with an integrating sphere placed in contact with the back of the sample (fused silica cuvette). The laser spot size on the cell was  $<0.5$  mm. The laser beam (He-Ne) is introduced for incidence angles of  $0^\circ$ ,  $30^\circ$ ,  $60^\circ$  and  $70^\circ$  with regard to the normal incidence (cuvette), which correspond to incidence angles into the sample of  $0^\circ$  (0 mrad),  $19.07^\circ$  (333 mrad),  $34.47^\circ$  (600 mrad) and  $37.89^\circ$  (661 mrad), respectively. The reflection coefficients, measured at the interface air-silica for incidence angles of  $0^\circ$ ,  $30^\circ$ ,  $60^\circ$  and  $70^\circ$ , are  $\sim 3.5\%$ ,  $\sim 2.2\%$ ,  $\sim 0.2\%$  and  $4.4\%$ , respectively. The specular reflection, measured at the interface silica-sample, was considerably less than 1% for all incidence angles. For experimental setup, see figure S1 of the supplementary information. The transmission coefficient ( $T(d)$ ) is defined as the ratio between total transmitted flux and the incident flux. The transmitted intensity is corrected through the reflection coefficient measured at the interface air-silica. The specular reflection, measured at the interface silica-sample is  $\ll 1\%$  for all incidence angles (negligible). The macroscopic absorption length was determined from the exponential decay of transmitted intensity ( $I_{TC}(d)$ ) for large  $d$  using a very small detection solid angle (for experimental setup, see figure S2 in the supplementary information).

*Propagating experiment:*

The intensity structure of a probe beam (He-Ne laser) was measured for each incidence angle after propagating a distance  $d=2.3$ mm through the scattering medium. A CCD camera collected the image of intensity profile  $I(x,y)$  at the sample output face. The input probe beam is  $<100$   $\mu\text{m}$  full-width at half-maximum (FWHM). In order to make statistic, a total of 30 images, collected for different input points, intensities and integration times, were recorded for each incidence angle  $\theta$ . The transmitted intensity is also corrected through the reflected intensity at the interface air-silica. The experimental setup for propagation experiment can be found in figure S3 of the supplementary information.

*Backscattering experiment:*

For the measurement of coherent backscattering, the sample is illuminated through a beam splitter that reflects 50% of laser intensity and with a parallel polarization to the incidence plane. The light backscattered is collimated by a lens  $L_3$  (25 mm focal length) and a CCD collects it. For each incidence angle, the intensity that enters the sample was corrected through the reflected intensity measured at the interface air-silica. The intensity of backscattering cones was also rescaled by the internal reflection at the interface silica-air (light coming out the cuvette). For experimental setups, see figure S4 in the supplementary information.

## Results and discussion

### *Transmission experiment*

In order to study the transport of light as a function of the incidence angle, transmission coefficient ( $T(d)$ ) was determined as a function of slab thickness ( $d$ ) for incidence angles ( $\theta$ ) of  $0^\circ$ ,  $30^\circ$ ,  $60^\circ$  and  $70^\circ$  with regard to the normal incidence. Figure 1a shows  $T(d; \theta)$  as a function of slab thickness for  $\theta$  equal to  $0^\circ$ ,  $30^\circ$ ,  $60^\circ$  and  $70^\circ$ .  $T(d; \theta)$  shows a quadratic decay  $T(d; \theta) \propto \beta(d_0 + d)^{-2}$  for all incidence angles, indicating localization transition<sup>2, 13, 31</sup> An increase in the decay rate is observed as the incidence angle is increased. For  $0^\circ$ ,  $T(d \rightarrow 0; 0^\circ)$  tends to be  $\sim 0.45$  for  $d=0$ , which is the expected value (supplementary information). For  $30^\circ$ ,  $T(d \rightarrow 0; 30^\circ)$  tends to be  $\sim 0.44$ , which is close to the expected value. However, for  $60^\circ$  and  $70^\circ$ ,  $T(d \rightarrow 0; \theta)$  tends to be values appreciably lower than expected  $\sim 0.37$  and  $\sim 0.35$ , respectively. This fact could be caused by an appreciable increase of absorbed energy near the input border ( $d \rightarrow 0$ ), which would imply that the intensity measured for  $d > 50 \mu\text{m}$  (measurement range) would be lower than expected. The latter might be explained through an increase of localization with the incidence angle (increase of internal reflection),<sup>30</sup> since absorbed energy ( $d \rightarrow 0$ ) must increase when localization increases.<sup>1, 13</sup>

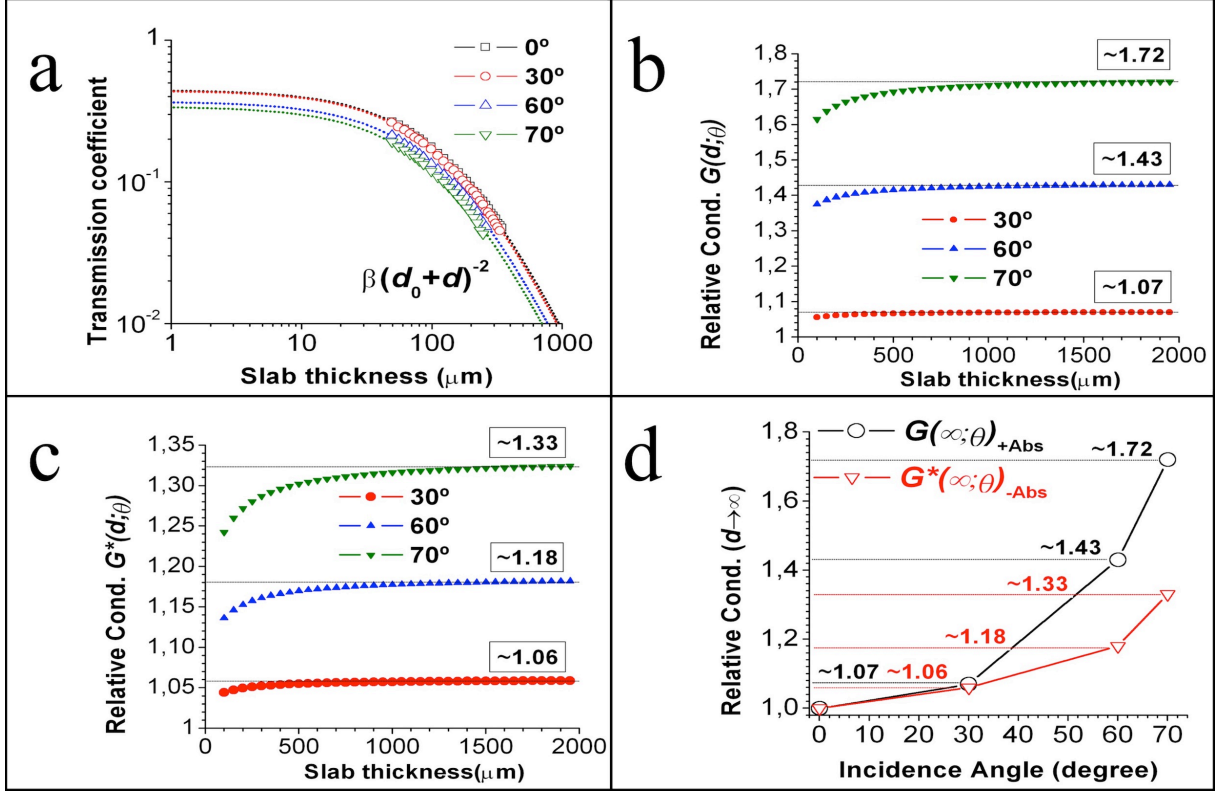


**Figure 1.** Transmitted total intensity vs incidence angle. a) Transmission coefficient for incidence angles  $\theta$  of:  $0^\circ$ ,  $30^\circ$ ,  $60^\circ$  and  $70^\circ$  as a function of slab thickness ( $d$ ). The black, red, blue and green dotted lines represent the fitting  $\beta(d_0 + d)^{-2}$  with experimental points for  $0^\circ$ ,  $30^\circ$ ,  $60^\circ$  and  $70^\circ$ , respectively. b and c) relative conductance as a function of  $d$ , b)  $G(d; \theta)$  with absorption and c)  $G^*(d; \theta)$  without absorption. d) Asymptotic values of relative conductance with absorption  $G(\infty; \theta)$  (black-circles) and without absorption  $G^*(\infty; \theta)$  (red-triangle) as a function of the incidence angle.

From  $T(d; \theta) = \beta(d_0 + d)^{-2}$  fittings, transport mean free path ( $l_T(d; \theta)$ ), extracted by the derivative of  $[T(d; \theta)]^{-1}$ ,  $\frac{\partial(T(d; \theta))^{-1}}{\partial(d)} \propto [l_T(d; \theta)]^{-1}$ , can be determined as a function of slab

thickness for each incidence angle. In figure 1b, the ratio  $\frac{\left(\frac{\partial(T(d; \theta))^{-1}}{\partial(d)}\right)}{\left(\frac{\partial(T(d; 0^\circ))^{-1}}{\partial(d)}\right)} = \frac{l_T(d; 0^\circ)}{l_T(d; \theta)}$ , which would

represent the relative conductance with regard to the normal incidence ( $G(d; \theta)$ ), is plotted as a

function of slab thickness. For very large  $d \rightarrow \infty$ ,  $G(d; \theta) = \frac{l_T(d; 0^\circ)}{l_T(d; \theta)}$  tends to be an asymptotic

value different for each incidence angle. This asymptotic value ( $G(\infty; \theta)$ ) increases as the

incidence angle is increased. However, an appreciable increase of absorbed energy at  $60^\circ$  and

$70^\circ$  would yield higher  $G(\infty; \theta)$  values than expected. Therefore, in order to estimate the

expected transmission curve for each incidence angle without “absorption” effect, the experimental points were fitted with  $T(d; \theta) = \beta(d_0 + d)^{-2} \times A$  function, where  $A$  constant would represent the losses of intensity by “absorption” ( $d \rightarrow 0$ ).  $A(\theta)$  values were fixed such that  $\beta / (d_0)^2 = 0.45$ , which is the expected  $T(d=0; \theta)$  value. The  $\frac{l_T(d; 0^\circ) \times A(\theta)}{l_T(d; \theta)}$  ratio, which would correspond the relative conductance without absorption effect ( $G^*(d; \theta)$ ), is shown in Figure 1c. Figure 1d shows the  $G(\infty; \theta)$  and  $G^*(\infty; \theta)$  increase when the incidence angle is increased.

In order to estimate the influential of the incidence angle on the absorption, transmitted intensity ( $I_{TC}(d; \theta)$ ) was measured as a function of slab thickness for large  $d$  using a very small detection solid angle. The macroscopic absorption length ( $l_{MA}$ ) can be determined from the inverse slope (log scale) of exponential decay ( $e^{-d/l_{MA}}$ ) (supplementary information). An  $l_{MA} \approx 104 \pm 2 \mu\text{m}$  was found for all incidence angles, revealing that  $l_{MA}$  is insensitive to the incidence angle. However, it is known that  $l_{MA}$  can be expressed as  $l_{MA} = (l_T \times l_{In})^{1/2}$ , where  $l_T$  and  $l_{In}$  are the transport and inelastic mean free path, respectively. Therefore, an increase in absorbed energy ( $d \rightarrow 0$ ) could be explained by a higher increase of  $l_T$  for  $d$  near zero ( $l_{T0}$ ) as the incidence angle is increased. The latter can be understood as that, an increase in the incidence angle provokes an appreciable increase in the internal reflection that leads to a localization increase.<sup>30</sup> In turn, an increase of localization results in an increase of  $l_{T0}$ , absorption ( $l_{In0}$  decrease) and  $n_{eff0}$  ( $d \rightarrow 0$ ). Of course,  $l_{In0}$  must be sufficiently greater than the microscopic coherence length,  $\xi_{Coh} \leq l_{In0}$ , such that absorption does not dominate the localization phenomenon. From the above results, an increase of localization (conductance decrease) and absorbed energy is inferred when the incidence angle is increased. Nevertheless, we must highlight that the data (figure 1c) could be potentially affected by an unphysical correction of absorption, which would yield an inaccurate relative conductance,

$G^*(\infty; \theta)$ . Additionally, although we have carefully measured the residual stray light, the data could be lightly spoiled by it. Therefore, in order to corroborate the above results (extrapolation for large  $d$ ), an additional experiment of propagation was performed.

### *Propagation experiment*

The intensity profile of a Gaussian probe beam was collected for each incidence angle after propagating a distance  $d=2.3\text{mm}$  through the sample. For incidence angles of  $0^\circ$ ,  $30^\circ$ ,  $60^\circ$  and  $70^\circ$ , normalized intensity profiles are displayed in figure 2a, 2b, 2c and 2d, respectively. The intensity profiles are not Gaussian; these could be fitted with a  $e^{-2(|r|/\sigma)^{1+\nu}}$  function (red solid line), where  $r$  is the radial distance of the beam center and  $0 < \nu < 1$ . Additionally, for large  $r$ , the intensity (profile) decreases more quickly when the incidence angle is increased, i.e. the intensity profile adopts a triangular shape. This effect is notable at the incidence angles of  $60^\circ$  and  $70^\circ$ . The latter could be explained by an appreciable increase of absorbed energy when the incidence angle is increased, which in turn, would be caused by an increase of localization ( $d \rightarrow 0$ ). Notice that, the intensity for large  $r$  must represent those photons with longer paths. For each incidence angle, the confinement of the beam at the output plane is quantified by the inverse participation ratio:  $P \equiv [\int I(x, y)^2 dx dy] / [\int I(x, y) dx dy]^2 = \frac{1}{\pi} [\int I(r)^2 dr] / [\int I(r) dr]^2$ , which has units of inverse area, and an effective width  $\omega_{\text{eff}} = (P)^{-1/2}$ . Figure 2e (left) shows the effective width as a function of the incidence angle, revealing an  $\omega_{\text{eff}}$  decrease as the incidence angle is increased above  $30^\circ$ . Figure 2e (right) shows the relative effective width with regard to the normal incidence,  $\frac{\omega_{\text{eff}}(0^\circ)}{\omega_{\text{eff}}(\theta)}$  (normalized width). For  $30^\circ$ ,  $\omega_{\text{eff}}$  decreases less to 1%, which is within the measurement error. However, a significant  $\omega_{\text{eff}}$  decrease is observed for  $60^\circ$  and  $70^\circ$ . This  $\omega_{\text{eff}}$  decrease is associated to the quicker decay of the intensity profile at large  $r$  when the incidence angle is increased.

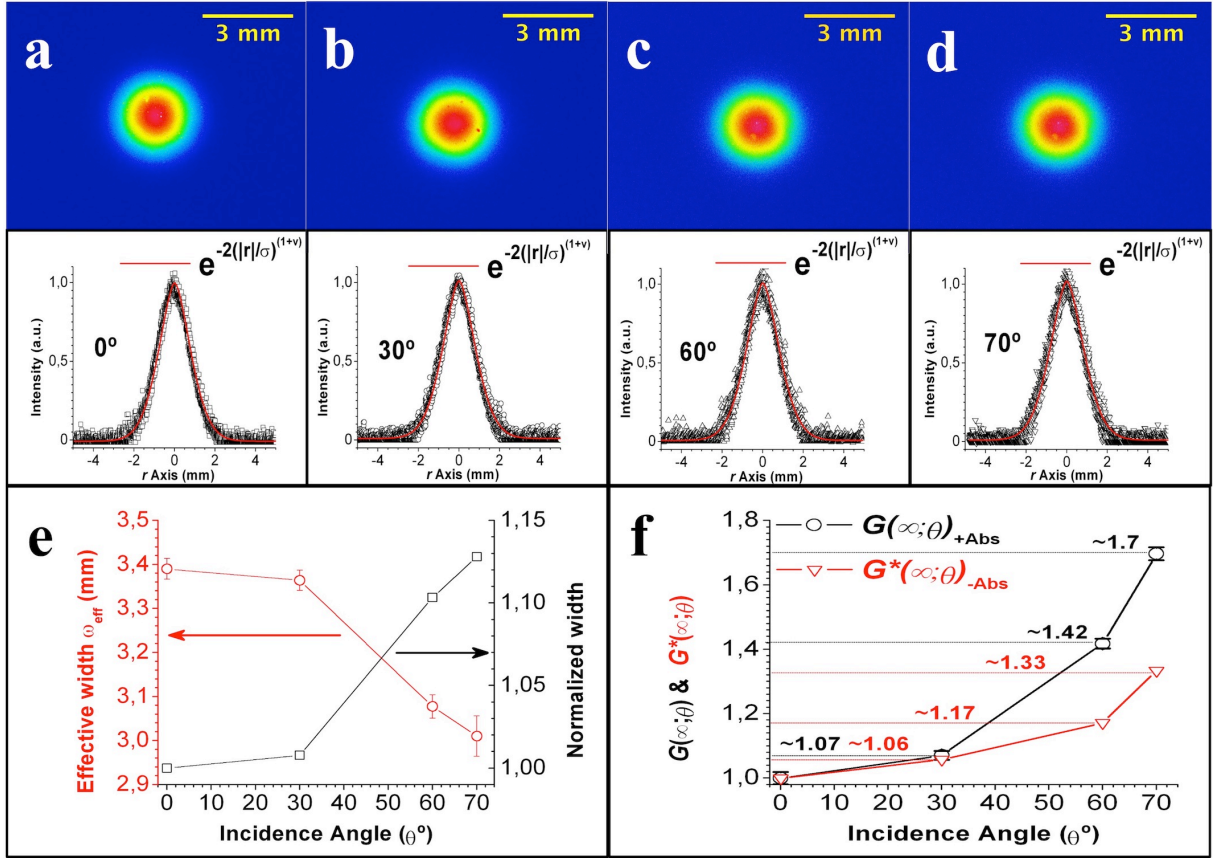


**Figure 2.** Experimentally measured intensity profiles at the sample output for incidence angles of: a)  $0^\circ$ , b)  $30^\circ$ , c)  $60^\circ$ , and d)  $70^\circ$ . The propagation length of probe beam was 2.3 mm and scale bar represents 3 mm. The intensity profiles are fitted to  $e^{-2(|r|/\sigma)^{1+\nu}}$ , where  $0 < \nu < 1$ . e) (left)  $\omega_{\text{eff}}$  vs incidence angle and (right) the relative effective width (normalized width). f)  $G(\infty; \theta)$  (black) and  $G^*(\infty; \theta)$  (red) as a function of the incidence angle. The error bars are the statistic standard deviation of relative intensity and effective width ( $\omega_{\text{eff}}$ ) in e) and f), respectively.

We must highlight that  $\omega_{\text{eff}}$  represents the mean conductance averaged by depth (from 0 up to 2.3 mm). Therefore, if  $\frac{\omega_{\text{eff}}(0^\circ)}{\omega_{\text{eff}}(30^\circ)} \approx 1$ , then for  $30^\circ$ , the asymptotic value of relative conductance without absorption effects ( $d \rightarrow \infty$ ),  $G^*(\infty; 30^\circ)$ , should be equal to the inverse of relative conductance at  $d=0$ ,  $(G^*(0; 30^\circ))^{-1}$ . Thus, let us introduce the following conjecture: For an incidence angle  $\theta$ , the asymptotic value of relative conductance ( $d \rightarrow \infty$ ) without absorption effects ( $G^*(\infty; \theta)$ ), should correspond with the localization increase at  $d=0$ ,  $(G^*(0; \theta))^{-1}$ , i.e.  $G^*(\infty; \theta) = (G^*(0; \theta))^{-1}$ . This would imply that the conductance averaged by depth,  $\omega_{\text{eff}}$ , should not change in the incidence angle, i.e. a  $\omega_{\text{eff}}$  decrease with the incidence angle would be

directly related to an increase of absorbed energy. Notice that  $l_{MA} = (l_T \times l_{In})^{1/2}$  does not depend on the incidence angle. This can be understood as that an  $l_T$  decrease for  $d \rightarrow \infty$ , when the incidence angle increases, should correspond to an equal  $l_T$  increase at  $d=0$ ,  $G^*(0; \theta) = (G^*(\infty; \theta))^{-1}$ .

In order to corroborate the asymptotic values of relative conductance with  $G(\infty; \theta)$  and without  $G^*(\infty; \theta)$  absorption, determined by extrapolation from the transmission experiment, the integrated intensity profiles ( $I(\theta) = \int I(x, y) dx dy$ ) was determined for each incidence angle  $\theta$ . In figure 2f,  $\frac{I(0^\circ)}{I(\theta)}$  and  $\frac{I(0^\circ)}{I(\theta)} \times \left(\frac{\omega_{eff}(0^\circ)}{\omega_{eff}(\theta)}\right)^{-2}$  ratio, which must represent the relative conductance with  $G(\infty; \theta)$  and without  $G^*(\infty; \theta)$  absorption (supplementary information), respectively, are plotted as a function of the incidence angle.  $G(\infty; \theta)$  and  $G^*(\infty; \theta)$  show similar behaviors to those extracted from the total transmission experiment.

In the above experiments, we showed a conductance decrease as the incidence angle is increased. This fact is attributed to a large increase of the internal reflection (input border) felt by the coherently backscattered photons (previously localized), due to the enhancement of the effective refractive index near the input border by localization. Therefore, the determination of this internal reflection, as a function of the incidence angle, becomes an imperative in order to confirm our hypothesis.

### *Backscattering experiment*

In order to determine experimentally the effective internal reflection felt by the coherently backscattered photons ( $IR$ ), the intensity of backscattering cone was measured as a function of the incidence angle. Figure 3a, 3b, 3c and 3d show the backscattering cone for incidence angles of  $0^\circ$  (0 mrad),  $30^\circ$  (524 mrad),  $60^\circ$  (1047 mrad) and  $70^\circ$  (1222 mrad), respectively. For experimental setup, see supplementary information. The specular reflection measured at the interface silica-sample for the photons that enter the sample is  $\ll 1\%$  for all incidence angles.

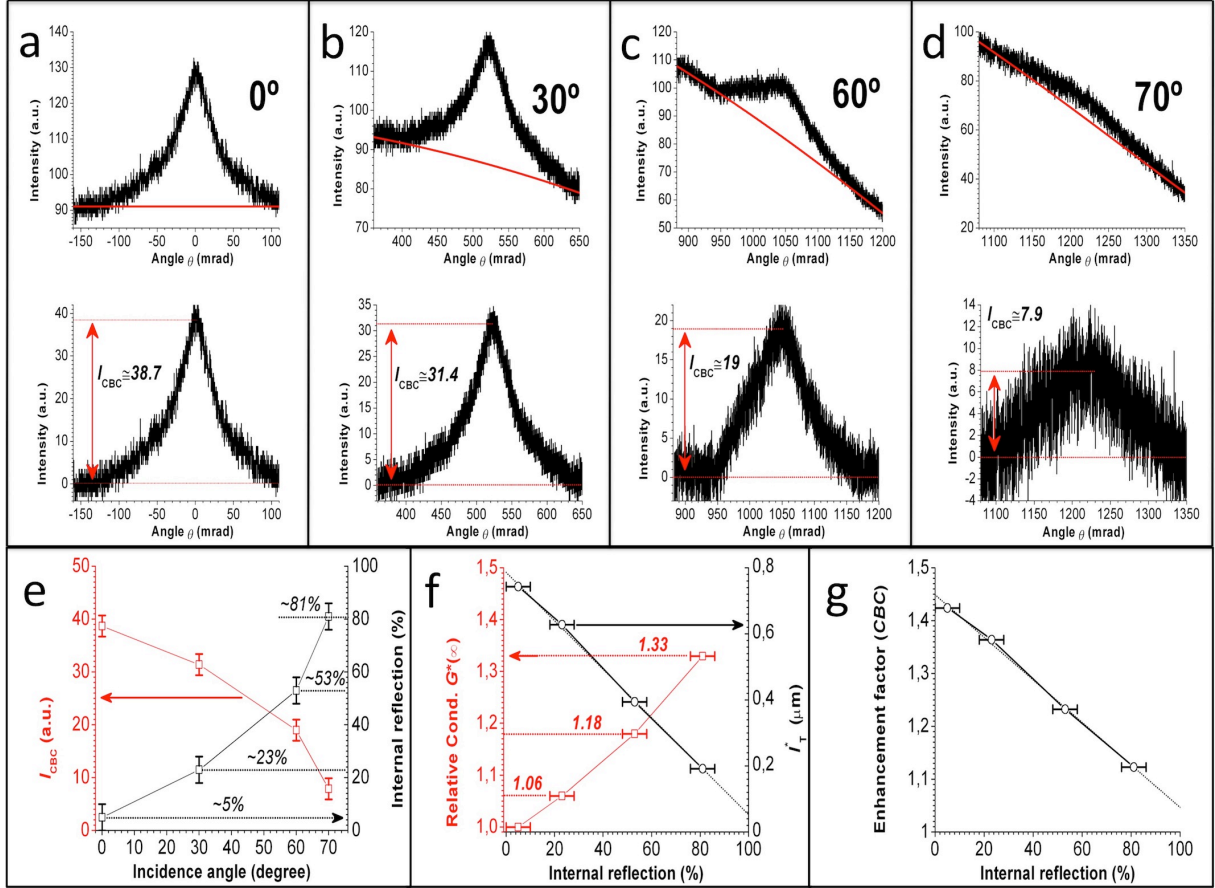


**Figure 3.** Coherent backscattering cones for incidence angles of: a) 0°, b) 30°, c) 60° and d) 70°. The red solid lines represent the background intensity (incoherently backscattered photons) taking into account the internal reflection at the interface silica-air (light coming out the cuvette). The coherent backscattering cones (below graphs) were extracted by subtraction of the background intensity (red lines). e) (left-red)  $I_{CBC}$  and (right-black)  $IR$  (%) as a function of the incidence angle. f) (left-red) asymptotic values of relative conductance without absorption ( $G^*(\infty)$ ), extracted from the total transmission and propagation experiments, and (right-black)  $I_T$  as a function of  $IR$  (%). g) The enhancement factor of backscattering cone as a function of  $IR$  (%). The black dotted lines at f) and g) represent linear fittings with the experimental points. Error bars correspond to the standard deviation of the intensity of the backscattering cone ( $I_{CBC}$ ) and the calculated  $IR$  (%).

From the intensity of backscattering cone, we extracted the effective internal reflection felt by the coherently backscattered photons (previously localized) at the interface sample-silica (photons coming out the sample). Notice that the backscattering cone must represent those photons previously localized. The background intensity, represented by the red solid lines (figure 3a-d), was determined by calculating the internal reflection (Fresnel's equations) for the incoherently backscattered photons at the interface silica-air (supplementary information). The internal reflection at the interface sample-silica must be negligible for the incoherently

backscattered photons ( $\ll 1\%$ ), since the refractive indexes of sample and silica felt by these photons are very close (1.53 and 1.46). The intensity of backscattering cone was also corrected by the internal reflection at the interface silica-air (photons coming out the cuvette). Figure 3e (left, red) shows the intensity of backscattering cone ( $I_{CBC}$ ) and (right, black)  $IR$  (%) as a function of the incidence angle. We calculated  $IR$  for each incidence angle,  $IR(\theta)$ , by the expression  $IR(\theta) = 1 - \frac{I_{CBC}(\theta)}{I_{CBC}^*}$ , where  $I_{CBC}(\theta)$  and  $I_{CBC}^*$  are the intensity of backscattering cone measured for each incidence angle  $\theta$  and the ideal intensity for null internal reflection, respectively. The internal reflection for the coherently backscattered photons at normal incidence ( $IR(0^\circ) \approx 5\%$ ) was determined considering an effective refractive index ( $d=0$ ) of 2.3 (supplementary information). From  $IR(0^\circ) \approx 5\%$ , we can determine  $I_{CBC}^*$  and, consequently,  $IR(\theta)$  for the other incidence angles.  $IR(\theta)$  values, determined for  $\theta$  of  $0^\circ$ ,  $30^\circ$ ,  $60^\circ$  and  $70^\circ$  are  $\sim 5\%$ ,  $\sim 23\%$ ,  $\sim 53\%$  and  $\sim 81\%$ , respectively, which are considerably higher than the specular reflection measured for the photons that enter the sample ( $\ll 1\%$ ) in the exact opposite direction. This indicates a non-reciprocal propagation of light, i.e. mirror-symmetry (parity symmetry) breaking. Notice that this large increase in the internal reflection undergone by the photons leaving the sample (coherently backscattered) would only be possible if the effective refractive index is largely enhanced. For a classical refractive index (1.53), the internal reflection for the photons leaving the sample (interface sample-silica) would be  $\ll 1\%$  for both polarizations and all incidence angles. A few pioneering theoretical and experimental studies have addressed the mirror-symmetry breaking in photonic crystal cavities,<sup>32,33,34</sup> however, no experimental evidence has been reported to date in a three-dimensional (3D) disordered optical medium. This phenomenon can be understood as that the photons that enter the sample feel a classical refractive index, but once are localized these photons feel an enhanced refractive index due to localization (successive elastic polarization of valence electrons to virtual states).

Figure 3f (left-red) shows  $G^*(\infty; \theta)$  values, determined from total transmission and propagation experiments, and (right-black) transport mean free path ( $l_T^*$ ), extracted by the half angle of backscattering cone,<sup>35</sup> as a function of  $IR$  (%). A simple model for internal reflection was taken into account for  $l_T^*$  correction (supplementary information).<sup>36,37</sup>  $l_T^*$  decreases monotonically as  $IR$  increases. We note that  $l_T^*$  does not tend to be zero when  $IR$  tends to be 100%. This fact could be because our system is at localization transition (crossover region), i.e. a percent of the photons does not localize. Figure 3g shows a monotonic decrease of the enhancement factor of backscattering cone as  $IR$  increases. These values of enhancement factor are considerably lower than the expected for a polarization parallel with regard to the incidence plane ( $\sim 1.8$ ). This effect can be explained by: i) the effective refractive index felt by the coherently backscattered photons (previously localized) is considerably higher than that felt by the incoherently backscattered photons (non-localized photons), which leads to a higher internal reflection for the coherently backscattered photons; ii) the perpendicular polarization of the coherently backscattered photons, with regard to original polarization (parallel to incidence plane), could increase as the incidence angle is increased. This latter could be because the internal reflection at  $\theta > 0^\circ$  is greater for perpendicular polarization ( $IR \rightarrow 100\%$ ). Consequently, those photons with perpendicular polarization with regard to the incidence plane would be localized preferably when the incidence angle is increased ( $\theta > 0^\circ$ ), since a localization increase is expected as internal reflection increases.<sup>30</sup> We do not have a clear interpretation for a possible change of polarization. This could be explained by an anomalous nonlinear increase of refractive index, due to the intensity increasing (energy increase) within the localized states.<sup>38</sup> The latter would give rise to a phase shift that continuously increases during the photon residence time ( $\tau_{e0}$ ). This phase accumulation can lead to an interference break, emitting photons away from the localized state. This nonlinear increase of the refractive index in a localized state (closed loop

path) would provoke like a Pockels effect, causing an elliptic polarization. A similar nonlinear phenomenon was theoretically addressed by Buttiker and Moskalets (disordered electronic media),<sup>39</sup> who proposed that when the energy of the localized state changes, the localized state can emit non-equilibrium electrons and holes propagating away from the localized state within the edge state which acts similar to a waveguide. The increase of localization in the incidence angle could be also interpreted as that photons from localized states, where the borders are involved (superficial localized states), that would be emitted by nonlinear effects (non-equilibrium)<sup>38,39</sup> can be again trapped in another superficial localized state, due to the increase of internal reflection. This latter implies that the density and residence time (Q factor) of superficial localized states would increase as internal reflection (incidence angle) increases, which can be inferred from the theoretical predictions of Mirlin<sup>28,29</sup> and Ramos and co-workers<sup>30</sup> in disordered electronic media. Notice that an increase of the internal reflection with the incidence angle would be remarkable, mainly for the coherently backscattered photons (previously localized), due to the enhanced refractive index that these photons would feel. For the incoherently backscattered photons, this effect would be considerably lower, since such photons would feel a classical refractive index. This means that the strong influence of the incidence angle over localization (conductance, absorption, refractive index), observed in the above experiments, would only be appreciable if the percentage of localized photons is considerably high, i.e. if the system is near localization. At diffusive regime, the conductance, absorption and refractive index must be insensitive to the incidence angle, since the internal reflection would change very little with the incidence angle. From the above results and ideas, we could infer that the conductance dependence with the incidence angle can be described through the transport of light near the input surface. The latter could be interpreted such that, the dependence of transport of light with the incidence angle must be determined by the superficial localized states, those where the borders are involved. A

detailed polarization study of the backscattering cone is called for, in order to determine the polarization of the coherently backscattered photons and its relationship with the incidence angle.

### **Conclusion**

Core-shell  $\text{TiO}_2@$ Silica nanoparticles at  $[140 \times 10^{10} \text{ NPs mL}^{-1}]$  in an ethanol solution allowed us to study the strong influence of the incidence angle on localization and associated phenomena. An increase of localization and absorbed energy are inferred as the incidence angle is increased. The increase of the effective internal reflection undergone by the coherently backscattered photons is proposed as likely cause of these phenomena. The measurement of the intensity of backscattering cone allowed us to determine the effective internal reflection felt by the coherently backscattered photons. From the experimental results, we inferred that an increase of the internal reflection (incidence angle) must provoke an increase of the density and residence time (Q factor) of superficial localized states, which is reflected in an increase of localization. This effect would only be appreciable if the percentage of localized photons is notably high, such that the effective refractive index would be largely enhanced near the input border, which in turn, would lead to an internal reflection strongly dependent of the incidence angle. The specular reflection at the interface silica-sample, measured for the photons that enter the sample, is considerably lower than the effective internal reflection determined for the coherently backscattered photons in the exact opposite direction, which indicates a breaking of the mirror-symmetry (parity symmetry). This latter opens a way to manufacture an all-optical diode. The results shown in this work could present important technological applications. For example, the texturing of input surface, which must lead to an enhancement of localization and absorbed energy, could open an avenue for the design and development of photonic devices based in strongly disordered optical media.

### **Acknowledgements**

We gratefully acknowledge financial support from FACEPE and CNPq (Brazil). Thanks to Professors Luis Poveda and Jorge Gabriel, for their thoughtful suggestions and discussions. We appreciate useful experimental support of Professors Mario Ugulino and Cid de Araujo. We extend additional thanks to Engineer Ricardo Acosta, for his corrections to the text.

### **Author Contribution**

All authors designed and performed the experiments and E.J-V guided the research and wrote the manuscript.

### **Conflict of interest**

The authors declare no competing financial interests.

### **Reference**

---

<sup>1</sup> Sajeev, John. Electromagnetic absorption in a disordered medium near a photon mobility edge. *Phys. Rev. Lett.* **53**, 2169–2172 (1984).

<sup>2</sup> Anderson, P.W. The question of classical localization A theory of white paint? *Phil. Mag. B* **52**, 505–509 (1985).

<sup>3</sup> John, S. Strong localization of photons near in certain disordered dielectric superlattices. *Phys. Rev. Lett.* **58**, 2486–2489 (1987).

<sup>4</sup> Sajeev, J. Localization of light. *Physics Today* **44**, 32. (1991).

<sup>5</sup> Wiersma, D. S., Bartolini, P., Lagendijk, A. & Righini, R. Localization of light in a disordered médium. *Nature* **390**, 671–673 (1997).

<sup>6</sup> Störzer, M., Gross, P., Aegerter, C. M. & Maret, G. Observation of the critical regime near Anderson localization of light. *Phys. Rev. Lett.* **96**, 063904 (2006).

<sup>7</sup> Sperl, T., Bührer, W., Aegerter, C. M. & Maret, G. Direct determination of the transition to localization of light in three dimensions. *Nature Photonics* **7**, 48–52 (2013).

<sup>8</sup> Scheffold, F., Lenke, R., Tweer, R. & Maret, G. Localization or classical diffusion of light? *Nature* **398**, 206. (1999).

<sup>9</sup> Scheffold, F. & Wiersma, D. Inelastic scattering puts in question recent claims of Anderson localization of light. *Nature Photonics* **7**, 934 (2013).

<sup>10</sup> van der Beek, T., Barthelemy, P., Johnson, P. M., Wiersma, D. S. & Lagendijk, A. Light transport through disordered layers of dense gallium arsenide submicron particles. *Phys. Rev. B: Condens. Matter* **85**, 115401. (2012).

<sup>11</sup> Sperl, T., Schertel, L., Ackermann, M., Aubry, G. J., Aegerter, C. M., Maret, G. Can 3D light localization be reached in 'white paint'? *New J. Phys.* **18**, 013039 (2016).

- 
- <sup>12</sup> Chabanov, A. A., Stoytchev, M., & Genack, A. Z. Statistical signatures of photon localization, *Nature* **404**, 850 (2000).
- <sup>13</sup> Jimenez-Villar, E., et al. Anderson localization of light in a colloidal suspension (TiO<sub>2</sub>@Silica). *Nanoscale* **8(21)**, 10938-10946 (2016).
- <sup>14</sup> Demirȯrs, A. F., Blaaderen, A. V., Imhof, A. Synthesis of eccentric titania-silica core-shell and composite particles. *Chem. Mater.* **21**, 979-984 (2009).
- <sup>15</sup> Abderrafi, K., Jimenez, E., Ben, T., Molina, S.I., Ibáñez, R., Chirvony, V., Martínez-Pastor, J. Production of nanometer-size GaAs nanocrystals by nanosecond laser ablation in liquid. *Journal of Nanoscience and Nanotechnology* **12**, 6774-6778 (2012).
- <sup>16</sup> Jimenez-Villar, E., Mestre, V., Oliveira P. C. & de Sá, G. F. Novel core-shell (TiO<sub>2</sub>@Silica) nanoparticles for scattering medium in a random laser: higher efficiency, lower laser threshold and lower photodegradation. *Nanoscale* **5**, 12512–12517 (2013).
- <sup>17</sup> Jimenez-Villar, E., et al. TiO<sub>2</sub>@Silica nanoparticles in a random laser: Strong relationship of silica shell thickness on scattering medium properties and random laser performance. *Appl. Phys. Lett.* **104**, 081909 (2014).
- <sup>18</sup> Skipetrov, S. E., Sokolov, I. M. Absence of Anderson localization of light in a random ensemble of point scatterers. *Phys. Rev. Lett.* **112**, 023905 (2014).
- <sup>19</sup> Rodriguez, E., et al. Fabrication and characterization of a PbTe quantum dots multilayer structure. *Physica E* **26**, 361 (2005).
- <sup>20</sup> Rodriguez, E., et al. All-optical switching device for infrared based on PbTe quantum dots. *Superlattices and Microstructures* **43**, 626-634 (2008).
- <sup>21</sup> Jimenez, E., Abderrafi, K., Abargues, R., Valdes, J. L., Martinez-Pastor, J. Laser-ablation-induced synthesis of SiO<sub>2</sub>-capped noble metal nanoparticles in a single step. *Langmuir* **26**, 7458-7463 (2010).
- <sup>22</sup> Jimenez, E., et al. A novel method of nanocrystal fabrication based on laser ablation in liquid environment. *Superlattices and Microstructures* **43**, 487–493 (2008).
- <sup>23</sup> Gonzalez-Castillo J. R., et al. Synthesis of Ag@Silica Nanoparticles by Assisted Laser Ablation. *Nanoscale Research Letters* **10(1)**, p9. (2015).
- <sup>24</sup> Fuertes, G., et al. Switchable bactericidal effects from novel silica-coated silver nanoparticles mediated by light irradiation. *Langmuir* **27**, 2826-2833 (2011).
- <sup>25</sup> Rodríguez, E., et al. SiO<sub>2</sub>/PbTe quantum-dot multilayer production and characterization. *Appl. Phys. Lett.* **86**, 113117 (2005).
- <sup>26</sup> Kellermann, G., et al. Structure of PbTe(SiO<sub>2</sub>)/SiO<sub>2</sub> multilayers deposited on Si(111). *Journal of Applied Crystallography* **43**, 385-393 (2010).
- <sup>27</sup> Campagnano, G. & Nazarov Yu. V.  $G_Q$  corrections in the circuit theory of quantum transport. *Physical Review B* **74**, 125307 (2006).
- <sup>28</sup> Mirlin, A.D. Spatial structure of anomalously localized states in disordered conductors *J. Math. Phys.* **38**, 1888 (1997).
- <sup>29</sup> Mirlin, A. D. Statistics of energy levels and eigenfunctions in disordered systems. *Physics Reports* **326**, 259-382 (2000).
- <sup>30</sup> Barbosa, A.L.R., Bazeia, D., Ramos, J.G.G.S. Universal Braess paradox in open quantum dots. *Physical Review E* **90**, 042915 (2014).

- 
- <sup>31</sup> Abrahams, E., Anderson, P. W., Licciardello, D. C. & Ramakrishnan, T. V. Scaling Theory of Localization: Absence of Quantum Diffusion in Two Dimensions. *Phys. Rev. Lett.* **42**, 673–676 (1979).
- <sup>32</sup> Maes, B., Bienstman, P., Baets, R. Switching in coupled nonlinear photonic-crystal resonators. *J. Opt. Soc. Am. B* **22**, 1778 (2005).
- <sup>33</sup> Maes, B., Soljacic, M., Joannopoulos, J. D., Bienstman, P., Baets, R., Gorza, S. P., Haelterman, M. Switching through symmetry breaking in coupled nonlinear micro-cavities. *Opt. Express* **14**, 10678 (2006).
- <sup>34</sup> Hamel, P., et al. Spontaneous mirror-symmetry breaking in coupled photonic-crystal nanolasers. *Nature Photonics* **9**, 311-315 (2015).
- <sup>35</sup> Akkermans, E., Wolf, P. E. and Maynard, R., Coherent backscattering of light by disordered media: analysis of the peak line shape, *Phys. Rev. Lett.* **56**, 1471-1474 (1986).
- <sup>36</sup> Lagendijk, A., Vreeker, R., de Vries, P. Influence of internal reflection on diffusive transport in strongly scattering medium, *Phys. Lett. A*, **136 (1–2)**, 81–88 (1989).
- <sup>37</sup> J.X. Zhu, D.J. Pine, D.A. Weitz. Internal reflection of diffusive light in random medium. *Phys. Rev. A* **44**, 3948-3959 (1991).
- <sup>38</sup> Jimenez-Villar, E., et al., Random lasing at localization transition in a colloidal suspension (TiO<sub>2</sub>@Silica), *ACS Omega*, DOI: 10.1021/acsomega.7b00086.
- <sup>39</sup> Buttiker, M., Moskalets, M. From Anderson Localization to Mesoscopic Physics. *Int. J. Mod. Phys. B* **24 (12n13)**, 1555-1576 (2010).